UNIVERSITY OF MISKOLC

FACULTY OF MECHANICAL ENGINEERING AND INFORMATICS
INSTITUTE OF MATERIALS SCIENCE AND TECHNOLOGY

SCIENTIFIC STUDENT CONFERENCE THESIS

OPTIMIZING CMT WELDING PARAMETERS FOR HIGH-STRENGTH STEEL JOINTS USING HIGH SPEED CAMERA ANALYSIS

WRITTEN BY:
Tanuj Namboodri
student of the Mechanical Engineering study program at MSc level

SUPERVISOR (S):
Dr. Raghawendra Pratap Singh Sisodia
Associate professor

Sahm Alden Abd AL AL
Ph.D. Student

Miskolc, 2023.

Declaration of authenticity

I, the undersigned Tanuj Namboodri, a student at the Faculty of Mechanical Engineering and Informatics of the University of Miskolc, declare and certify with my signature that I have prepared this thesis myself, I have carried out the examinations described therein, unless I indicate otherwise, and I have achieved the results described myself. I used data and information only from the sources listed in the bibliography. Any part that I have taken from another source, either verbatim or in the same sense, but reworded, is clearly marked with the source.

Miskolc, 07.11.23

signature

Statement of the supervisor

I, the undersigned, Dr. Raghawendra Pratap Singh Sisodia the lecturer in the Institute of Material Science and Technology at the University of Miskolc I consider the Scientific Student thesis (TDK thesis) entitled *Optimizing CMT Welding Parameters for High-Strength Steel Joints Using High Speed Camera Analysis* to be suitable for submission.

Miskolc, 07. 11. 2023.

…….
signature

Table of Contents

1. INTRODUCTION 5
2. MATERIAL PROPERTIES 7
3. METHODOLOGY 8
4. RESULTS 14
5. CONCLUSION 21
6. REFERENCES 22

Abstract

Welding technology plays an important role in various industries ranging from automotive to aerospace. The ability to produce strong, durable joints in materials such as high-strength steels (HSSs) is critical for automotive industries and products that fulfil the required technical criteria. Cold Metal Transfer (CMT) welding has developed as a potential welding technology, with various benefits such as lower heat input, less distortion, minimal spatter, and precise control over the welding process. Cold Metal Transfer (CMT) welding technology, a high-precision welding method known for its suitability in welding high-strength materials like high strength steels (HSSs), Al-alloys etc. However, optimising CMT welding settings for high-strength steel joints is still a challenging task. During the study, utilising the high-speed camera footage and mechanical testing to draw conclusions about the optimal welding parameters for high-strength steel. Analysing the challenges encountered during the welding process and, in real time, using high-speed cameras to help in understanding and mitigating these challenges.

1. Introduction

Over the last decade, there has been a significant advancement in the development and commercialization of High-strength steels (HSSs), specifically engineered to assist automotive manufacturers in achieving weight reduction goals while maintaining stringent occupant safety standards[1]. In the domain of automotive structural applications, the utilization of high-strength steels has seen a notable uptick due to their durability, crash resistance, and manufacturing convenience[2]. The advancements in the automotive industry encompass the evolution of HSSs, characterized by an optimal blend of essential attributes such as remarkable strength, ductility, formability, and weldability. This unique combination enables the reduction of vehicle weight while simultaneously enhancing crash performance[3]. This innovative approach has spurred the development of high-strength dual-phase (DP) steels, which exhibit a microstructure comprising a ferrite matrix interspersed with martensite islands. DP steels have found widespread application in the automotive sector due to their exceptional multifaceted properties, including strength, ductility, formability, and weldability[4]. These qualities have significantly contributed to improving the strength-to-weight ratio of vehicles and reducing CO_2 emissions. The nomenclature "DP1000" signifies a dual-phase steel with a "double-phase" microstructure, while the number 1000 correspond to the minimum guaranteed tensile strength values in megapascals (MPa). Martensite is an exceedingly hard phase characterized by a body-centred tetragonal structure, whereas ferrite exhibits a relatively softer phase with a body-centred crystal structure. The utility of HSSs, extends beyond the automotive sector, HSSs have gained extensive practical use in engineering structures and heavily stressed construction elements, including cranes, heavy-duty trucks, and bridges. This adoption is attributed to their exceptional combination of both high strength and toughness, which makes them ideal for such demanding applications, it’s worth noting that these steel structures can be assembled through either the fabrication of hot-rolled steel sections or the welding of high-strength steel plates [5].

The ongoing developments in high-strength steels (HSSs) are largely being driven by the changing landscape of end-user demands, especially within the automotive industry[3]. Car manufacturers are grappling with significant shifts in regulations that now impose stringent requirements for safety and fuel efficiency. These new regulations necessitate specific combinations of strength and formability characteristics in materials. In Figure 1., there is a

classification of both traditional and advanced high-strength steels, primarily falling into the realm of thin plates. This graphical representation depicts the tensile strength and elongation percentages of various steel grades. What's evident from the figure is that these categories are not entirely distinct but instead exhibit overlaps. Additionally, each group aligns along three characteristic curves, with their characteristic values represented by the symbol "k_m" as a material constant[4]

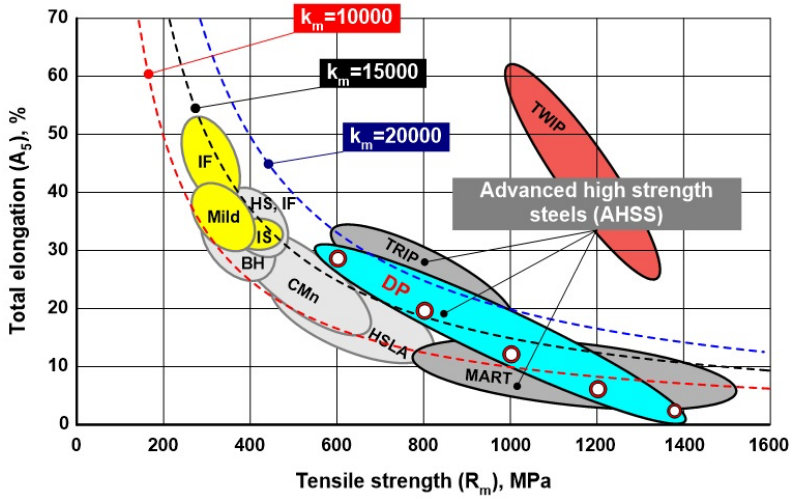

Fig 1. HSSs developments over the period[4]

In article [6], several welding difficulties of HSSs are emphasised, as high-strength steels have evolved, the importance of welding technology has surged, playing a crucial role in enhancing the ability to effectively join these materials to ensure they function optimally. In the automotive industry, this has become particularly prominent in the assembly of materials like dual-phase (DP) steels, which are in demand for their superior strength, quality, lightweight properties, passenger safety, and cost-effectiveness. This technology is indispensable for achieving the desired outcomes in the modern automotive sector[7].Weldability of HSSs can cause the decreasing of the strength and the toughness, another problem of weldability is the susceptibility of some welds to cold cracking, softening and hardening behaviour[8]. As a result, it is crucial to investigate the weldability of these HSSs using various advanced welding technological methods, and cold metal transfer (CMT) welding technique was chosen for this study.

Cold Metal Transfer (CMT) welding stands as an innovative approach to the joining of HSSs representing an enhanced iteration of the traditional Gas Metal Arc Welding (GMAW) methods which was developed by Fronius of Austria in 2004, In CMT, a distinctive manoeuvre involves retracting the filler metal wire after a momentary short circuit. This welding technique is particularly well-suited for connecting thin metal sheets and plates[9]. By adopting CMT, one can effectively reduce issues like spatter, joint distortion, and the need for extensive post-weld clean-up. Notably, CMT has enabled the successful bonding of aluminium and steel. Moreover, it provides the advantage of precise arc length control, which can be easily managed through mechanical means. The torch produces heat, which in turn raises the temperature of the plates or sheets intended for fusion[10]. Simultaneously, a wire is introduced into the torch, where it undergoes melting before uniting the sheets or plates through fusion. Various categories of CMT includes, CMT Pulse, CMT Advanced, CMT Pulse Advanced and CMT – Dynamic. The primary goal of this research is to optimise CMT welding parameters for HSS

DP1000 steel joints with 1mm thickness, and thus two different welding speeds (40 cm/min and 50 cm/min) were selected for the study. Analyse and compare the mechanical properties (microhardness, tensile strength, and bending) as well as the microstructural properties (optical microscope). Also, a high-speed camera and synchronous electrical signal acquisition device were used to examine droplet transition characteristics.

2. Material Properties

In this research, DOCOL uncoated cold-rolled steel sheet DP1000 is used as base material (BM), manufactured by Swedish Steel (SSAB), with a thickness of 1 mm. The DP1000 steel was selected due to its favourable characteristics for the welding process and increasing demand of it in automotive industry which leads to the problem of hardening & softening in weldability. DP1000 grade steel has1000 MPa guaranteed tensile strength, that can be welded by matching filler material, Union X96 with diameter of 1.2 mm. The motivation of using X96 filler metal wire was to provide matching strength, to avoid softening and cross section reduction in the weld as happening in the laser beam welding[4], [11], [12]. By using this matching filler material, the goal is to preserve and replicate the strength properties of DP1000 in the welded joint, thus maintaining structural integrity and performance[13].

Table 1 presents the chemical composition of the base material (BM), DP1000, and filler metal (FM), providing a comprehensive overview of the elemental components and their respective concentrations within this specific steel alloy. This information is crucial for understanding the material's properties and its suitability for various applications. In contrast, Table 2, provides a comprehensive listing of the mechanical properties associated with the BM and FM.

Table 1. The chemical composition of the base material and filler metal (weight%)[4]

Material designation	**C**	**Si**	**Mn**	**P**	**S**	**Cr**	**Ni**	**Mo**
DP1000	0.132	0.19	1.5	0.1	0.003	0.03	0.03	0
***Union X96 (Ø1.2 mm)	0.1	0.81	1.94	0.015	0.011	0.52	2.28	0.53
Material designation	**V**	**Ti**	**Cu**	**Al**	**Nb**	**B**	**N**	**CE**
DP1000	0.01	0	0.01	0.041	0.14	0.0002	0.004	0.39
***Union X96 (Ø1.2 mm)	<0.01	0.06	0.06	< 0.01	N/A	N/A	N/A	0.79

Table 2. Mechanical properties of base materials & filler metal[4]

Material designation	**$R_{p0.2}$ (MPa)**	**R_m (MPa)**	**A (%)**	**(HV0.2)**	**CVE, J (at -40 °C)**
DP1000	821	1074	9.5	227	N/A
***Union X96 (Ø1.2 mm)	≥ 930	≥ 980	≥ 14.0 (A_5)	N/A	-50 °C: ≥ 47; 20 °C: ≥ 80

The microstructure of the DP1000 base material was examined through optical microscopy and scanning electron microscopy (SEM), as shown in Fig. 2(a) and Fig. 2(b), respectively[14].

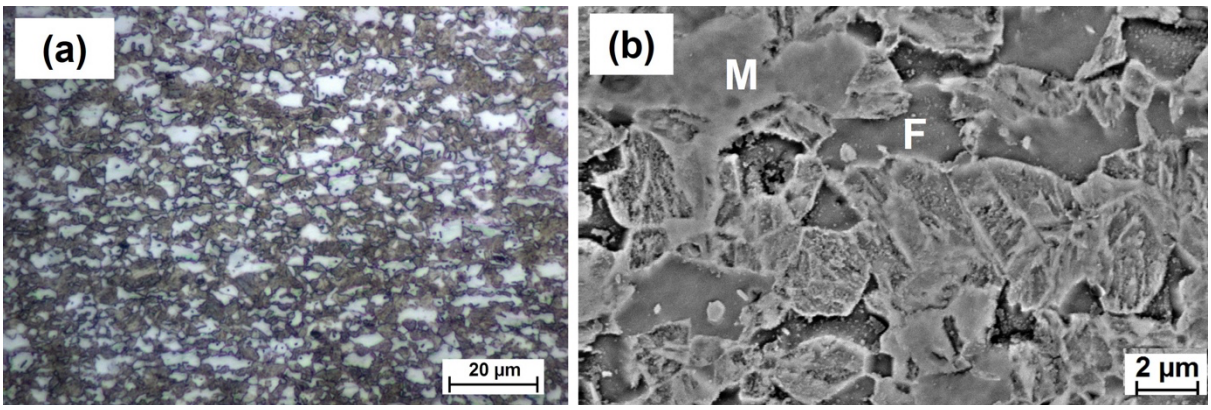

Fig 2. Base material microstructure, (a) Optical micrograph M=1000×, (b) SEM micrograph M=5000× (2% Nital); M= Martensite, F= Ferrite

3. Methodology

3.1. Sample Preparation

In this research for trial, a total of 20 specimens were cut, each measuring 10 x 3 units, for initial testing. Specimens were precisely joined together using varying wire feed rates, voltage, and current. To ensure precise alignment of the edges, edge preparation using finish milling prior to the welding process are performed. Additional cleaning of the samples is done by applying acetone and emery paper to eliminate any dust and surface oxide, ensuring a pristine surface for further procedures. The selection of these parameters was guided by the visual results obtained during the initial welding experiments, cutting the transverse cross section of the welded joint, and examining the penetration depth through polishing and etching.

3.2. Clamping Device Preparation

Clamping preparation is crucial in welding to securely hold the workpieces in place. Proper clamping ensures accurate alignment, minimizing distortion in the final weld. It helps maintain the desired joint geometry and promotes consistent, high-quality welds.

3.3. Setting of Camera and Transient Recorder

The camera is strategically positioned to capture the welding process, ensuring a comprehensive visual record that is synchronized with the transient recorder, which collects real-time data such as voltage and current fluctuations during the welding operation. This synchronization is essential for detailed analysis, allowing researchers to correlate visual observations with the precise electrical parameters of the CMT welding process[15].

3.4. Experimental Setup

CMT welding is known for its ability to create high-quality and precise welds, making it suitable for various applications, including automotive and aerospace industries. The setup ensures control and accuracy throughout the welding process. (CMT) welding is an advanced welding technique that involves a specific setup for the various components mentioned.

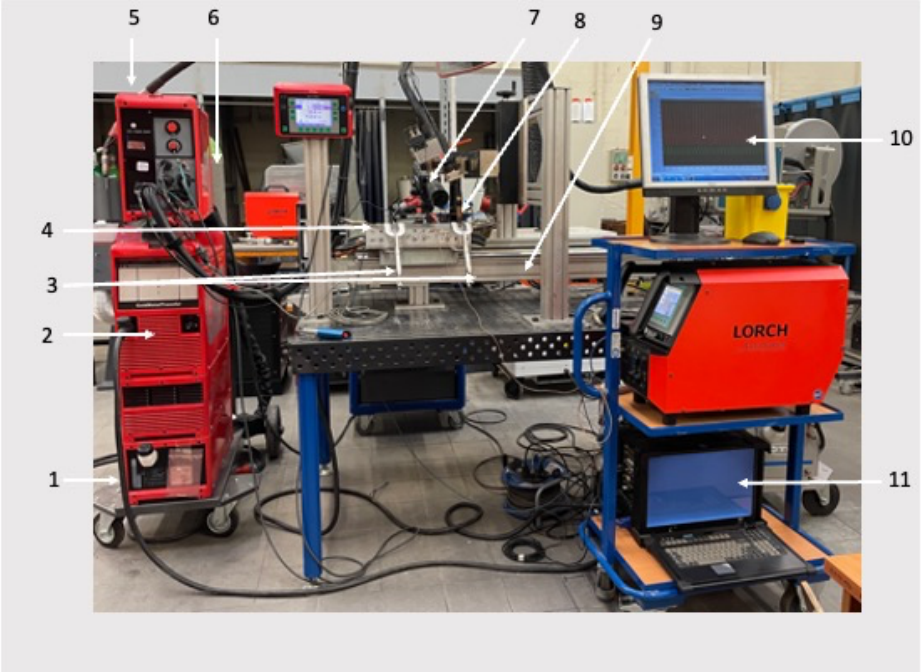

Fig 3. – Experimental welding setup

1.Coolant: Provides cooling for the welding torch and other heat-sensitive components to prevent overheating. *2. Power Source:* Supplies the electrical current required for the welding process, with precise control over voltage and amperage. *3. Clamps:* Used to secure the workpiece in the desired position during welding. *4. Workpiece*: The material or parts to be joined through welding. *5. Wire Feed Unit:* Supplies the consumable welding wire at a controlled rate for the welding process. *6. Gas Cylinder*: Contains shielding gas, such as argon or a mix of gases, to protect the weld area from atmospheric contamination. *7. High-Speed Camera*: Monitors and records the welding process with high frame rates to assess weld quality and make real-time adjustments. *8.* Welding Torch: The tool that holds the welding wire and directs the heat to the workpiece, often equipped with a special mechanism for the CMT process. *9.* Work Bed: The surface where the workpiece is positioned for welding. *10*. Monitor: Displays real-time data, including welding parameters and camera footage, for the welder to monitor and adjust the process as needed. *11.* Oscilloscope: Measures and displays electrical signals and waveforms, which can be essential for diagnosing and optimizing the welding process.

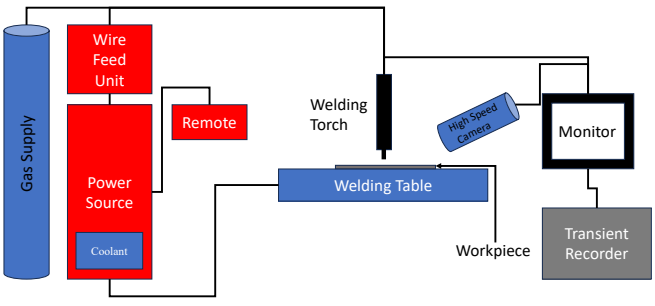

Fig *4.* Schematic of CMT welding setup.

Table 3 provides a comprehensive overview of the welding parameters employed in the study, specifically applied to 10 different samples. These parameters are essential for understanding the conditions under which the welding experiments were conducted. The constant gas flow rate used in all 10 samples was 18 liters/minute, ensuring a consistent shielding gas environment for the welding process. The torch angle, set at 90 degrees for all samples, remained unchanged throughout the experiments. This angle is critical for directing the heat and the welding arc onto the workpiece in a uniform manner. A consistent tip distance of 12.7 mm was maintained for all samples. This distance represents the gap between the welding torch's tip and the surface of the workpiece, influencing the arc's behavior and the weld's quality. However, one crucial parameter was intentionally varied, the rate at which the welding wire was fed into the welding process varied among the samples. This parameter has a significant impact on the deposition of the filler material, affecting the weld's integrity and dimensions. The welding current, measured in amperes, was adjusted differently for each sample. Current is a key factor in controlling the heat input, which directly affects the melting and bonding of the base materials [16], [17] . The welding voltage and current which are measured in Volts and Ampere was automatically modified by machine while changing the wire feed rate. Voltage and current plays a pivotal role in determining the arc's stability and heat distribution during the welding process. The Eq. (1) was used to calculate the heat input during deposition:

$$E = \eta \frac{UI}{v} \tag{1}$$

where U in Volt, I in ampere, v in mm/s, η= 0.8[18].

The data in Table 3 serves as a critical reference for understanding the experimental conditions and their impact on the weld quality.

Table 3 – Experiment data with different wire feed rate, current, voltage & welding speed

Sample no.	Wire Feed	Current	Voltage	Welding Speed	Tip Distance	Heat input
	m/min	I	V	cm/min	mm	kJ/mm
1	1.2	63	11.5	25	12.7	0.11
2	1.7	74	12.8	50	12.7	0.09
3	1.7	75	12.8	70	12.7	0.06
4	1.7	74	12.7	90	12.7	0.05
5	1.4	66	12.9	60	12.7	0.06
6	1.7	73	13.4	40	12.7	0.11
7	1.7	75	12.5	45	12.7	0.1
8	1.7	75	12.5	46	12.7	0.09
9	1.7	74	13.2	45	12.7	0.1
10	1.7	74	13	25	12.7	0.18

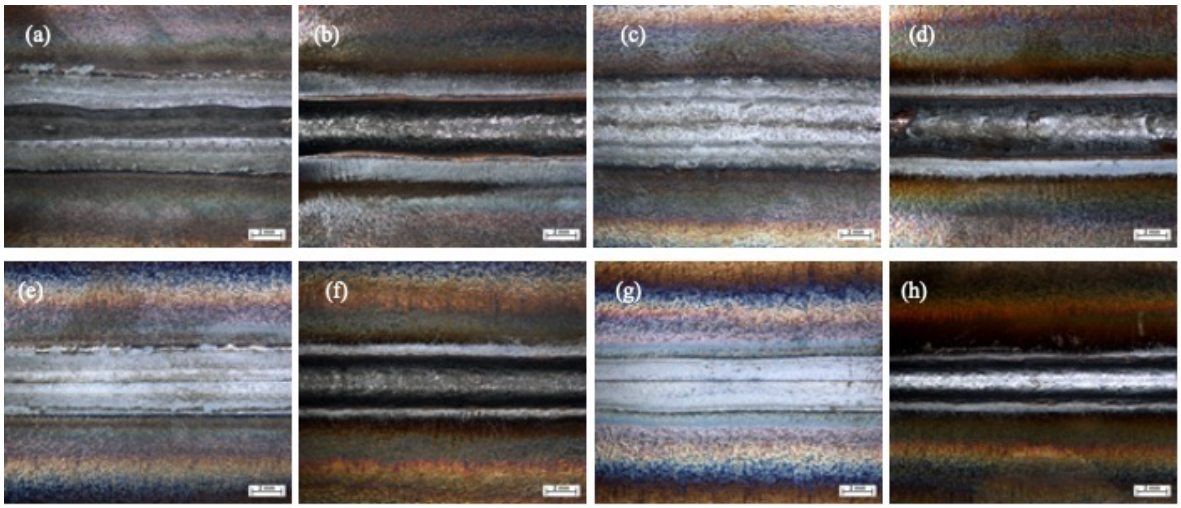

Fig 5. (a) root side, (b) face side of sample no. 1, (c) root side, (d) face side of sample no. 2, (e) root side (f) face side of sample no. 3, (g) root side, (f) face side of sample no. 4 [Refer Table no. 3]

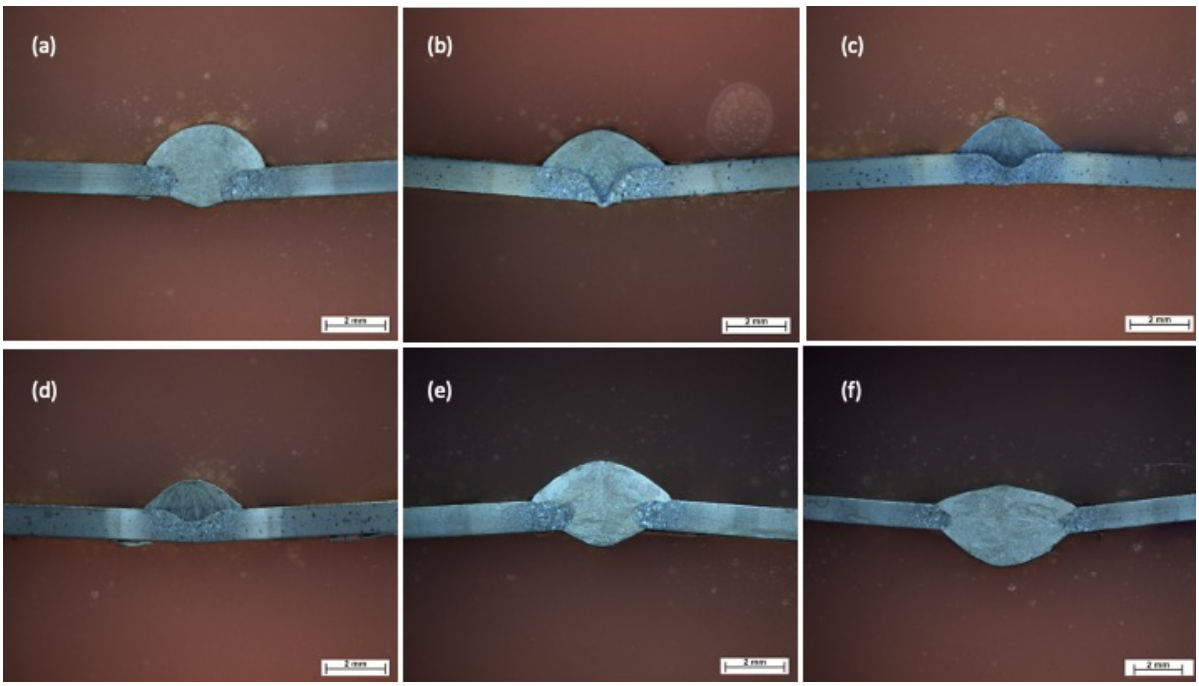

Fig 6. Weld cross section (a) Sample no. 1, (b) Sample no. 2, (c) Sample no. 3, (d) Sample no. 4, (e) Sample no. 6, (f) Sample no. 10 [Refer Table 3]

In Sample No. 1, the wire feed was set at 1.2 m/min while the welding speed was 25 cm/min. In Figure (a), full penetration is clearly evident. In Sample No. 2, although full penetration was not achieved, the weld almost reached full penetration, as indicated in Figure (b). Sample No. 3 displayed around 50% penetration, as depicted in Figure (c), and Sample No. 4 exhibited minimal penetration. In Sample No. 6, a weld with full penetration and good quality was observed, as shown in Figure (e). Sample No. 10 also achieved full penetration, although there is an excess of material on the root side, as illustrated in Figure (f). The welding parameters utilized for all ten welded samples are comprehensively presented in Table 3.

Subsequently, a series of butt-welding experiments were conducted on set of samples, the details of which are comprehensively outlined in Table 3. This table serves as a valuable reference, encapsulating the specific parameters used for these subsequent welding trials. From this broader set of experiments, two results were carefully handpicked to be included in the final phase of the study, which is shown in Table 4, representing the most promising and relevant outcomes for further analysis and consideration.

After conducting a series of meticulous experiments, two specific sets of parameters emerged as the most promising candidates for further investigation and testing in the final phase of the study. These parameters were carefully selected based on their performance and relevance to the research objectives as presented in Table 4. Sample no. 2 and Experiment no. 6 were identified as the two most suitable candidates for this pivotal final experiment and subsequent testing. The decision to focus on these two experiments was made after a rigorous evaluation of their outcomes.

Table 4 – Optimal parameters for final welded joints

Sample No.	Wire Feed	Current	Voltage	Welding Speed	Tip Distance	Heat input
	m/min	I	V	cm/min	mm	kJ/mm
6.1	1.7	73	13.4	40	12.7	0.117
2.1	1.7	74	12.8	50	12.7	0.09

Prior to the welding experiment, we prepared specimens by cutting them from a DP1000 sheet, resulting in pieces measuring 300 mm × 150 mm, which were intended for creating a butt-welded joint in accordance with the EN 15614-11 standard. To ensure pristine surfaces, the edges of the specimens underwent cleaning using emery paper and acetone, effectively removing any surface oxide. 3D model for welded sheet is represented in Fig.7

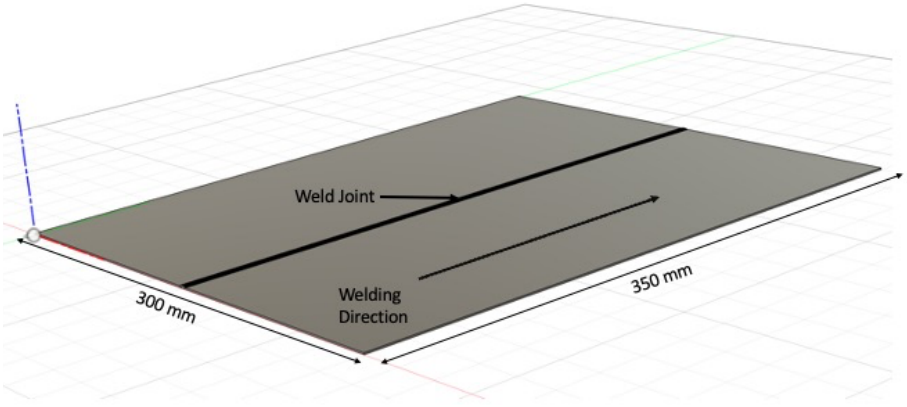

Fig 7. 3D Model of the welded sheets

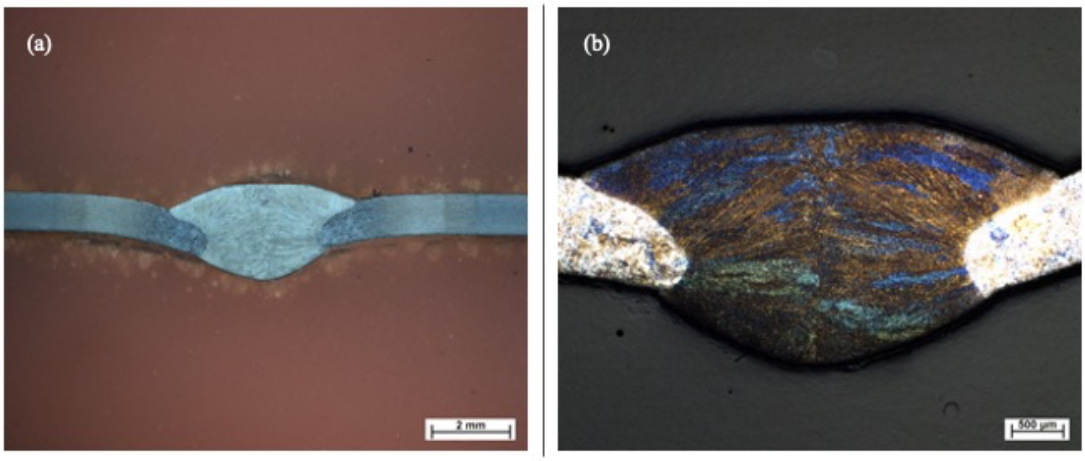

Fig 8. (a) Weld cross section 10× (b) Weld cross section 25× for sample no. 6.1

Figure 8. (a) provides a cross-sectional view of a weld, showcasing the results of the welding experiment conducted with the parameters for Sample Number 6.1. These parameters include a wire feed rate of 1.7 m/min, a welding speed of 40 cm/min, a current setting of 73 A, and a voltage level of 13.4 V. The image offers a detailed visual representation of the internal structure of the weld and penetration depth, allowing for a closer examination of the welding outcome under these specific conditions.

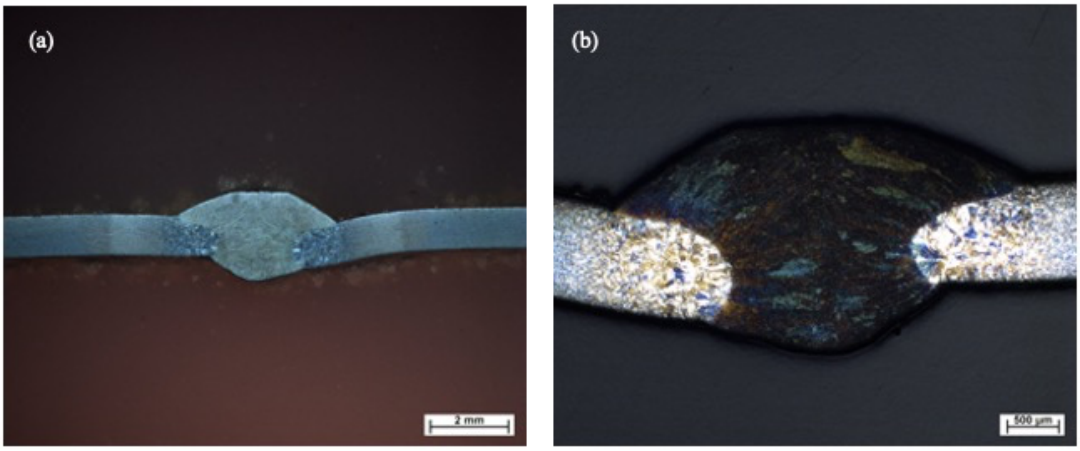

Fig 9. (a) Weld cross section 10× (b) Weld cross section 25× for sample no. 2.1

Figure 9(a) provides a cross-sectional view of a welded joint, illustrating the results of a welding experiment conducted with the parameters specified for Sample Number 2.1 from table no. 5. These parameters include a wire feed rate of 1.7 m/min, a welding speed of 50 cm/min, a current setting of 74 A, and a voltage level of 12.8 V. This image offers a detailed visual insight into the internal structure and the penetration depth of the weld, allowing for a comprehensive examination of the welding outcome achieved under these specific conditions.

In both welded parts full penetration can be seen for both parameters used described in Table 4. In Fig 8(a) more material is collected on the root side and for Fig (9) the appropriate amount of material was collected on both face and root side.

4. RESULTS

A comprehensive quality assessment was conducted on the welded samples according to standard EN 15614-1, encompassing a series of meticulous examinations and tests as shown in Fig 10. These evaluations encompassed visual inspections, in-depth thorough microstructure examinations, precise transverse tensile testing, meticulous bending tests, and hardness testing, collectively ensuring a robust evaluation of the sample's overall quality and structural integrity.

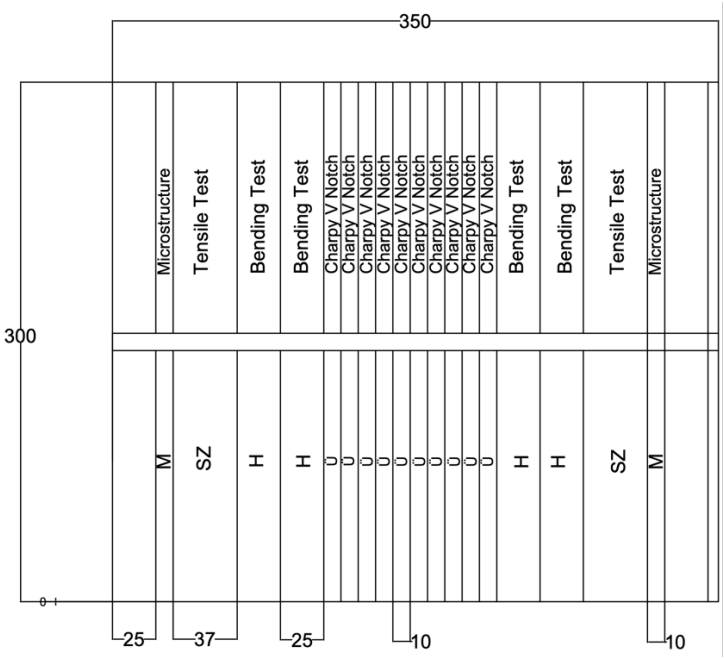

Fig 10. – Schematic representation of specimen for testing

4.1. Metal Transfer

The welding process employed a stationary welding gun, and all welds were executed in the flat position. This arrangement ensured that the high-speed video camera remained fixed in relation to the welding wire, arc, and molten weld pool, allowing for precise monitoring and analysis. The power source generated specific waveforms designed to create and control small molten droplets, which were subsequently detached from the welding wire. This detachment was achieved by using a low current in conjunction with the mechanical retraction motion of the wire.

In Fig 11 and 12 graphical representation illustrates the typical current waveform observed during Cold Metal Transfer (CMT) welding. The fundamental parameters governing this waveform include: Boost current (I_b), Wait current (I_w), Necking current (I_n), Detachment current (I_d), Boost duration (t_b), Necking time (t_n), Detachment time (t_d). The necking time (t_n), and detachment time (t_d). collectively constitute short circuit time (t_s) [18] . Fig 11 and 12 also describes the image collected by high-speed camera which clearly describes the steps involved in the welding process.

CMT welding for sample no. 6.1 is illustrated with Fig. no. 11, the parameter of welding is described in Table no. 4, Similarly, sample no. 2.1 is illustrated in Fig no. 12, different steps involved can be seen during the welding understand the process which helps researchers to understand the effect of changing parameter.

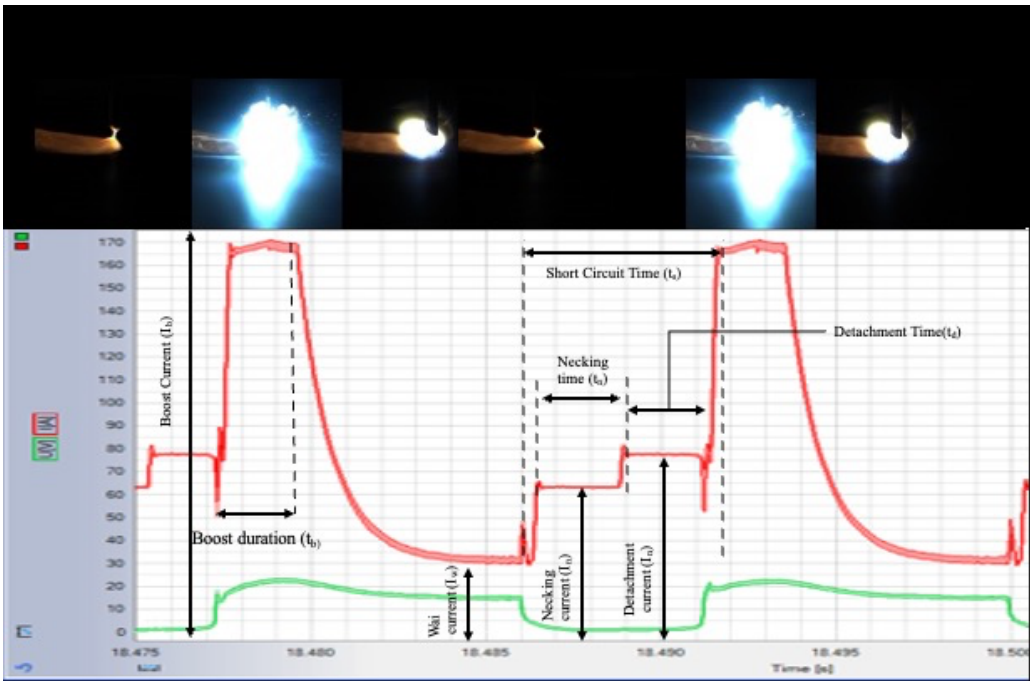

Fig 11. Metal transfer through high speed camera and current waveform of CMT welding sample no. 6.1

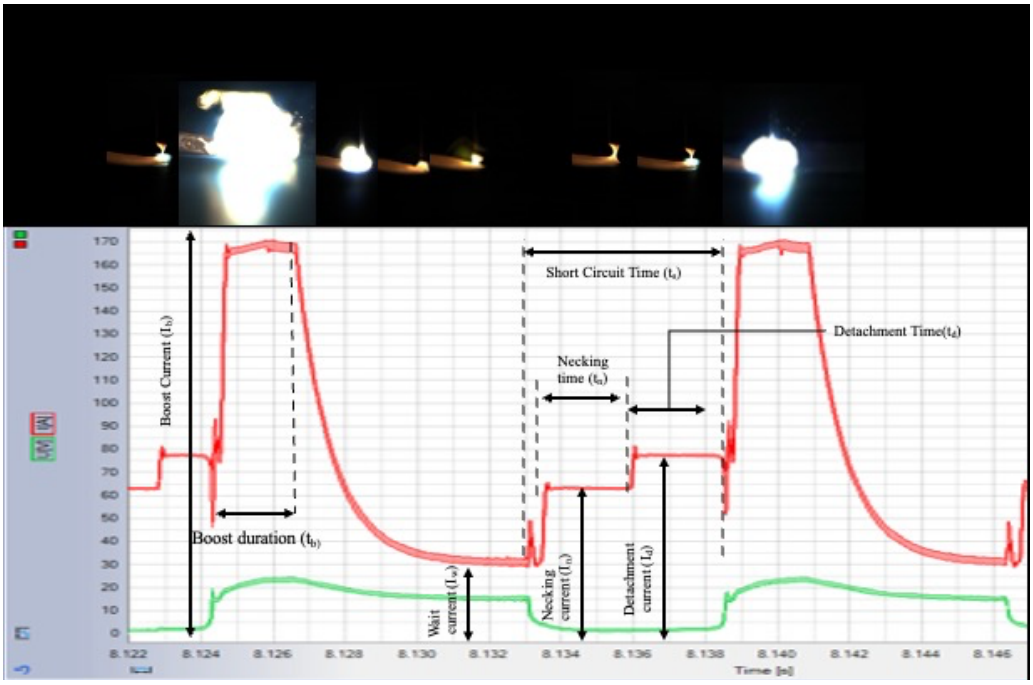

Fig 12. Metal transfer through high speed camera and current waveform of CMT welding sample no. 2.1

4.2. Hardness

Microhardness tests were conducted in adherence to ISO 9015-2 standard procedures for welded joints, and the results for Sample Number 6.1. The Vickers micro hardness tests (ISO 9015-2) were done by a Mitutoyo MVK-H1 Microhardness tester across the etched cross section of the welded sample with a load of 200 g for a 10 s dwell time. The micro indentations were taken corresponding to various regions within the welded specimen, including the BM,

the HAZ, and the FZ. The locations and results of these macro indentations are illustrated in Figure (13). This process allowed for an assessment of the hardness characteristics across the different regions of a CMT-welded specimen of DP1000 steel[3].

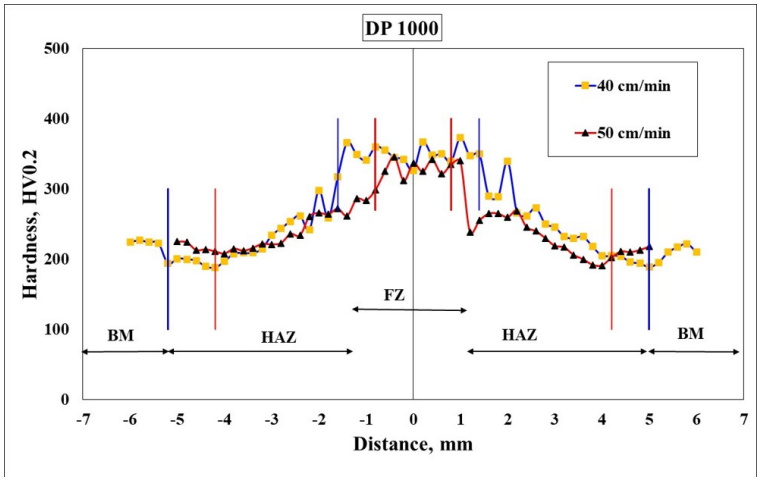

Fig 13. Microhardness distribution across the transverse cross-section of the welded joints.

The average hardness value measured in FZ and HAZ for the sample 6.1 are 349 and 238 HV0.2 respectively; for sample no 2.1, the average hardness value measured in FZ and HAZ are 328 HV0.2 and 241 HV0.2. The maximum or peak hardness was observed in CGHAZ of sample 6.1 which was 373 HV0.2. From the figure 13, it is clearly evident that the with lower welding speed (40 cm/min) and higher heat energy, the hardness of the FZ and HAZ is higher comparison to the higher welding speed (50 cm/min) and lower energy. The higher energy level and lower welding speed lead to a higher heat input. This means that a larger volume of the material is exposed to elevated temperatures for a longer duration during welding. Consequently, the slower cooling rate in the HAZ and fusion zone results in the formation of a microstructure that is less prone to hardening and can lead to higher hardness.

4.3. Microstructure

The microstructural examination was carried out using an OM (Axio Observer D1m (Zeiss) inverted microscope). Figure 14 illustrates the fusion zone with ma (FZ) and coarse grain heat-affected zone (CGHAZ) in the welded component. In Fig. 14(a), FZ mainly constitutes martensite for sample number 6.1, while (b) showcases the coarse grain martensitic structure for the same sample. Similarly, (c) presents the FZ with , and (d) exhibits the coarse grain for sample number 2.1. [19]

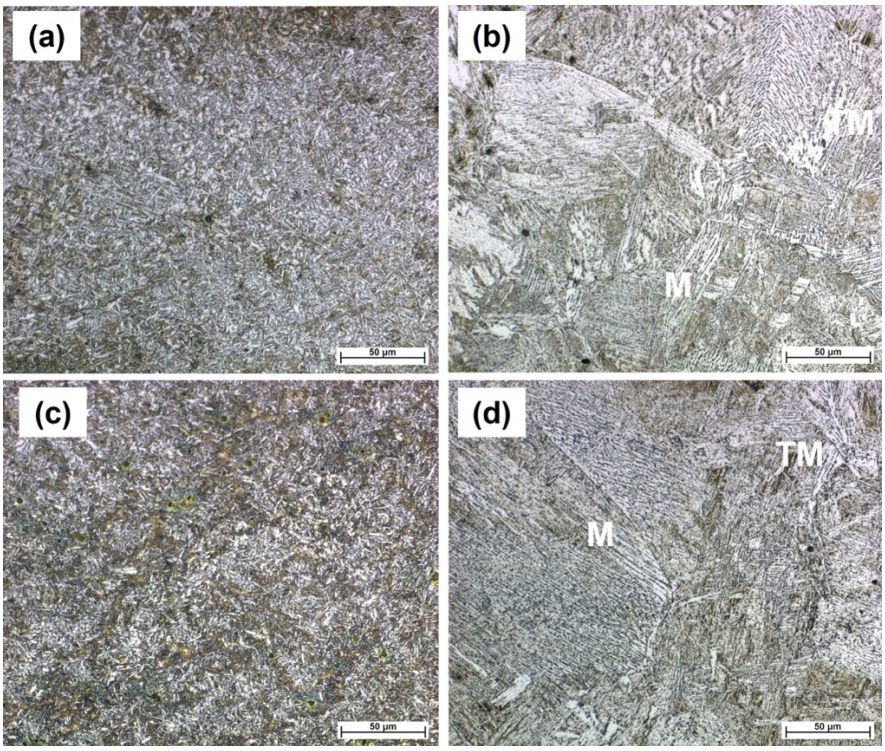

Fig 14. Top, 40 cm/min (a) FZ (b) CG ; Bottom, 50 cm/min (c) FZ (d) CG

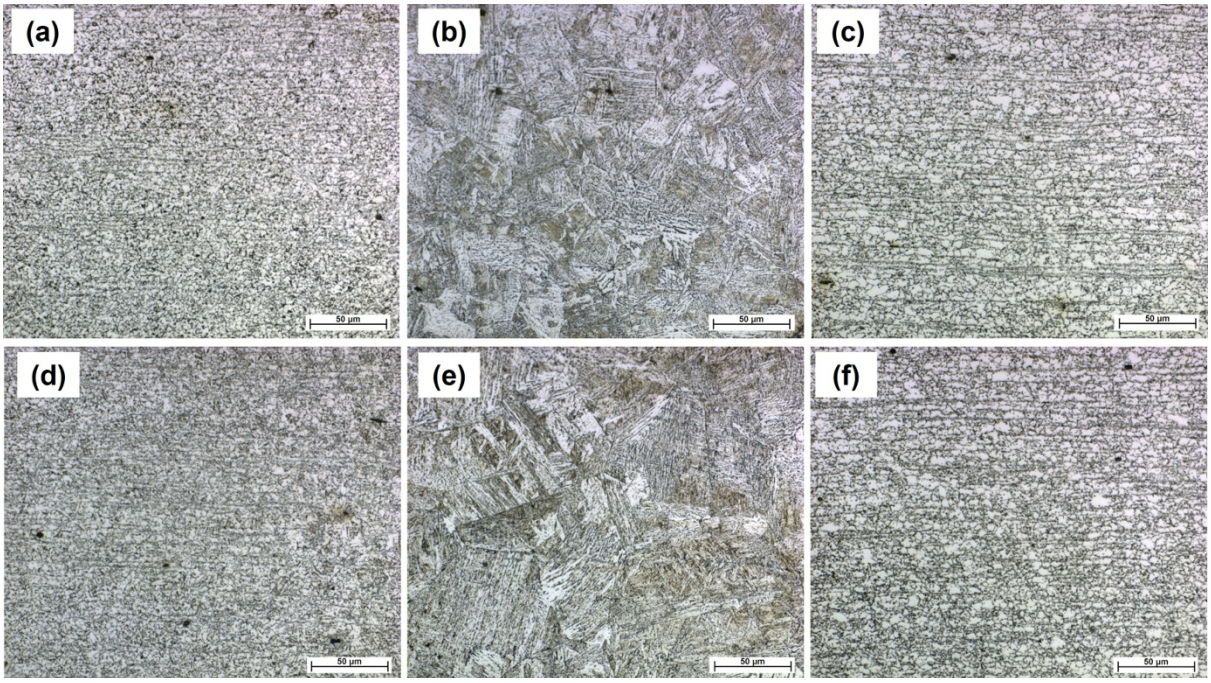

Fig 15. Top, 40 cm/min (a) FGHAZ, (b) ICHAZ, and (c) SCHAZ; Bottom, 50 cm/min (d) FGHAZ, (e) ICHAZ, and (f) SCHAZ

As depicted in Figure 14 and 15, the heat-affected zone (HAZ) can be subdivided into different regions: the coarse-grained HAZ (CGHAZ), fine-grained HAZ (FGHAZ), intercritical HAZ (ICHAZ), and sub-critical heat-affected zone (SCHAZ).

When examining the optical micrographs of the base materials, the ferrite components appear in white, and in the SEM images, they exhibit deeper etching compared to the martensite grains.

With respect to the CGHAZ, it can be inferred that a martensitic microstructure with a lathe-like appearance typically forms, and this aligns with the observed hardness peaks (Fig. 13). The slower cooling rate allows for more time for diffusion and microstructural changes to occur. Instead of rapid formation of hard martensite (which can lead to high hardness), the microstructure may evolve differently.

4.4. Transverse Tensile Test

The tensile test was carried out at room temperature using the MTS 322 tensile testing machine to determine the ultimate tensile strength of all welded specimens. The tensile test was performed at a rate of 0.2 mm/s. The comparative transverse tensile test results of CMT welded joints at 40 cm/min and 50 cm/min are presented in Table 5.

Table 5. Tensile properties of CMT welded DP1000 welded joints.

Welding speed (cm/min)	Sample No.	Force (kN)	Fracture location	Tensile strength (MPa)	Avg. tensile strength (MPa)
40	1a	18	HAZ	707	713
	1b	18	HAZ	718	
	1c	18	HAZ	713	
50	2a	20	HAZ	779	777
	2b	20	HAZ	777	
	2c	20	HAZ	776	

The results show a decrease in the tensile strength in both the CMT-welded joints at 40 cm/min and 50 cm/min. The BM tensile strength, according to the supplier material data sheet, was 1074 MPa. However, the reduction in strength in a welded joint with 40 cm/min was about 34%, and in a welded joint with 50 cm/min, it was 26%. However, the increase in tensile strength was observed when welding speed was increased from 40 cm/min to 50 cm/min, and it was about 9%. From Table 5 and Figure 17, it can be observed that there was an increase in tensile strength with the increase in welding speed and a decrease in energy input for the CMT-welded joint at 50 cm/min during the transverse tensile tests. However, further investigation is required with different combinations of the optimal parameters with full penetration to achieve the tensile strength closer to BM.

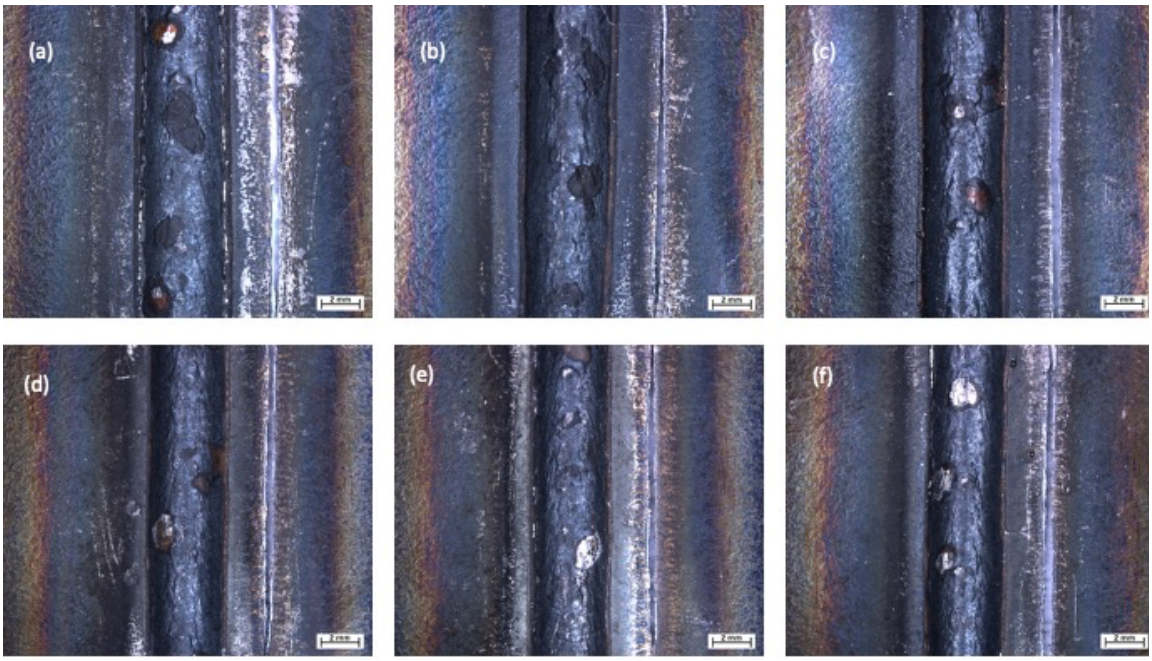

Fig 16. (a), (b), (c) Transverse tensile test sample number 6.1; (d), (e), (f) Transverse tensile test sample number.

From the Fig 16, it has been clearly observe that the fracture took place in HAZ specially SCHAZ areas of the weld for the tested specimens in each category. This is due to the microhardness reduction which causes softening behaviour close to the boundary between the HAZ and the BM.

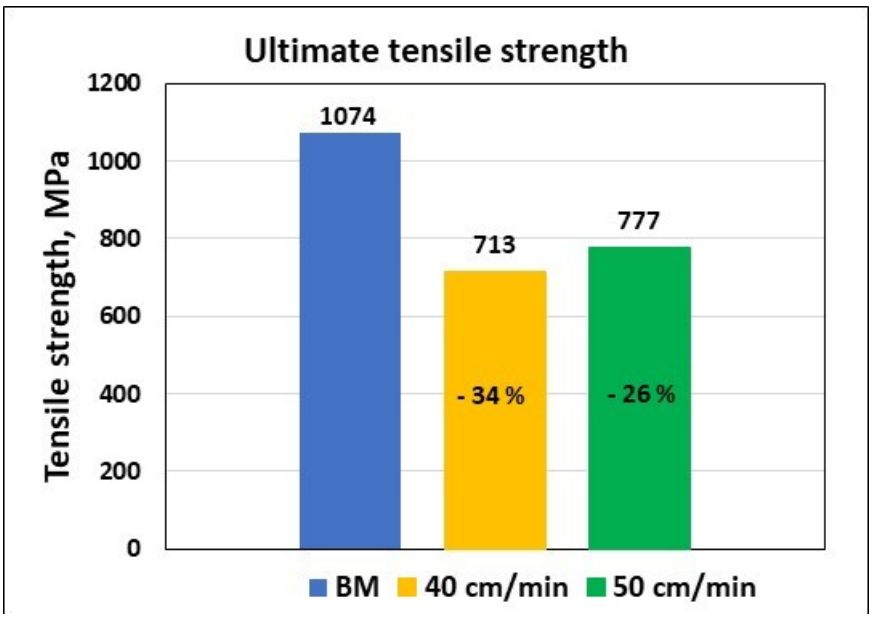

Fig 17. Ultimate tensile strength chart

4.5. Bending Test

The bending test was conducted on welded joints using MTS322 testing equipment at a rate of 1 mm/s with the aim of detecting potential cracking during deformation caused by weld imperfections in both the face and root regions of the weld. To assess the bending characteristics of these joints, a three-point bend test in accordance with EN 5173 was executed

on both the face side and root side, as depicted in Fig. 18 and 19 For this test, a rectangular specimen measuring 200 mm in length, 25 mm in width, and 1 mm in thickness was used. The indenter possessed a diameter of 4 mm, while the fixed support roller had a diameter of 10 mm, with a support span (the distance between the rollers) of 20 mm.

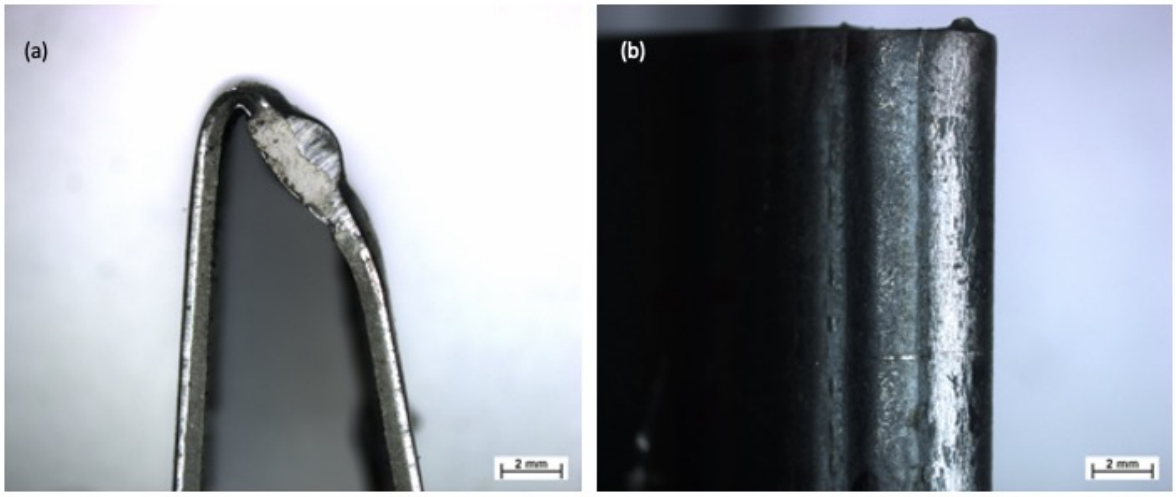

Fig 18. Bending test sample no. 6.1, (a) Front view (b) Back view.

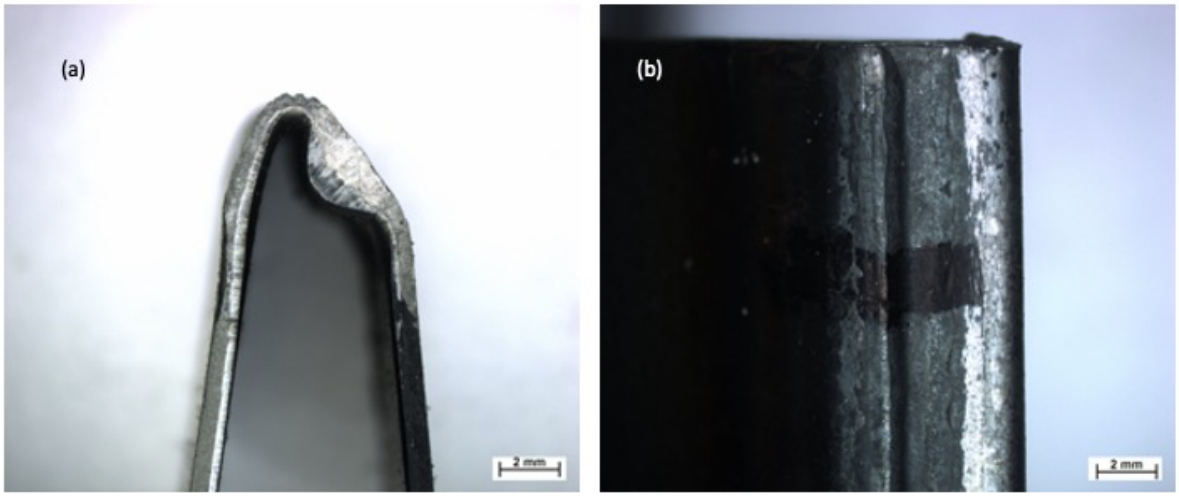

Fig 19. Bending test sample no. 2.1, (a) Front view (b) Back view

In the conducted bending test, it was observed that neither of the tested samples, as depicted in Figure 18 (a), (b) and Figure 19 (a), (b), exhibited any fractures or cracks. This unequivocal result underscores the remarkable plastic properties of the welded joints, as no structural flaws or weaknesses were detected during the examination. The bending test conclusively demonstrated the outstanding integrity and durability of the specimens on both the face and root sides, reaffirming the quality of the welding process.

Based on the findings presented in the forementioned study, it can be deduced that the welding parameters used in sample no. 2.1 yield significantly more favourable results when compared to sample no. 6.1. These parameters are, therefore, deemed to be well-suited for achieving robust weldability in the context of High-Strength Steels (HSSs), particularly in the case of DP1000 steel grades.

Furthermore, the bending tests conducted on the welded joints have revealed commendable plastic properties, indicating that the welds possess the capacity to withstand deformation without exhibiting any structural weaknesses.

In addition, the tensile strength analysis has demonstrated that sample no. 2.1 outperforms sample no. 6.1 in terms of tensile strength, reaffirming the superior mechanical characteristics of the former. This not only highlights the advantages of the selected welding parameters but also underscores their suitability for applications requiring high tensile strength in DP1000 steel grades.

5. CONCLUSION

1) The present study and observed phenomena can be attributed to the complex interplay of welding parameters, resulting microstructural changes, and their influence on mechanical properties.

2) The image collected by high-speed camera which clearly describes the steps involved in the CMT welding process and the arc characteristics.
3) The BM microstructures consist of martensite and ferrite. The CGHAZ mainly constitutes of coarser martensite.

4) The average hardness value measured in FZ and HAZ for the sample with 40 cm/min are 349 and 238 HV0.2 respectively; for sample with 50 cm/min, the average hardness value measured in FZ and HAZ are 328 HV0.2 and 241 HV0.2. The maximum or peak hardness was observed in CGHAZ of sample with 40cm/min which was 373 HV0.2.

5) The reduction in strength in a welded joint with 40 cm/min was about 34%, and in a welded joint with 50 cm/min, it was 26%. However, the increase in tensile strength was observed when welding speed was increased from 40 cm/min to 50 cm/min, and it was about 9%.

6) The slower cooling rate at the higher energy level can lead to a microstructure that, despite being harder, may exhibit slightly lower tensile strength due to the presence of more ductile phases.

7) To achieve the desired balance of mechanical properties in the welded joint, it's essential to optimize the welding parameters, including energy level, welding speed, tip to workpiece distance etc. The goal is to control the microstructure in a way that maximizes both strength and toughness for the specific application.

6. REFERENCES

[1] M. Shome and M. Tumuluru, “Introduction to welding and joining of advanced high-strength steels (AHSS),” *Welding and Joining of Advanced High Strength Steels (AHSS)*, pp. 1–8, Jan. 2015, doi: 10.1016/B978-0-85709-436-0.00001-1.

[2] K. P. Imlau and T. Heller, “New steel solutions for the werldwide car industry,” in *Steel Research International*, Verlag Stahleisen GmbH, 2007, pp. 180–184. doi: 10.1002/srin.200705877.

[3] R. P. S. Sisodia, M. Gáspár, and L. Draskóczi, “Effect of post-weld heat treatment on microstructure and mechanical properties of DP800 and DP1200 high-strength steel butt-welded joints using diode laser beam welding,” *Welding in the World*, vol. 64, no. 4, pp. 671–681, Apr. 2020, doi: 10.1007/s40194-020-00867-6.

[4] “UNIVERSITY OF MISKOLC FACULTY OF MECHANICAL ENGINEERING AND INFORMATICS HIGH ENERGY BEAM WELDING OF ADVANCED HIGH STRENGTH STEELS PHD THESES Raghawendra Pratap Singh Sisodia ISTVÁN SÁLYI DOCTORAL SCHOOL OF MECHANICAL ENGINEERING SCIENCES TOPIC FIELD: ENGINEERING MATERIALS SCIENCE, PRODUCTION SYSTEMS AND PROCESSES TOPIC GROUP: MATERIALS ENGINEERING AND MECHANICAL TECHNOLOGY”, doi: 10.14750/ME.2021.051.

[5] H. Lin, Y. Hu, S.-T. Qian, and M. Sulaiman, “Application of Continuous Strength Method in high strength steel sections,” *ce/papers*, vol. 4, no. 2–4, pp. 1612–1616, 2021, doi: https://doi.org/10.1002/cepa.1463.

[6] M. Gáspár, R. P. S. Sisodia, and A. Dobosy, “Physical Simulation-Based Characterization of HAZ Properties in Steels. Part 2. Dual-Phase Steels,” *Strength of Materials*, vol. 51, no. 5, pp. 805–815, Sep. 2019, doi: 10.1007/s11223-019-00128-y.

[7] G. A. Kunitsyn, S. V. Denisov, A. V. Gorbunov, A. G. Vetrenko, A. I. Brus’Yanina, and E. V. Zharkov, “Production of high-strength steel sheet for the auto industry,” *Steel in Translation*, vol. 38, no. 7, pp. 585–588, Jul. 2008, doi: 10.3103/S0967091208070231.

[8] M. Tisza, “Biographical notes: Miklós Tisza obtained his MSc in Mechanical Engineering from the Technical University for Heavy Industry in 1972 and his PhD from the University of Miskolc in 1977,” 2013.

[9] D. Srinivasan, P. Sevvel, I. John Solomon, and P. Tanushkumaar, “A review on Cold Metal Transfer (CMT) technology of welding,” *Mater Today Proc*, vol. 64, pp. 108–115, Jan. 2022, doi: 10.1016/j.matpr.2022.04.016.

[10] R. Nishimura, N. Ma, Y. Liu, W. Li, and T. Yasuki, “Measurement and analysis of welding deformation and residual stress in CMT welded lap joints of 1180 MPa steel sheets,” *J Manuf Process*, vol. 72, pp. 515–528, Dec. 2021, doi: 10.1016/j.jmapro.2021.10.050.

[11] R. P. S. Sisodia and M. Gáspár, “An Approach to Assessing S960QL Steel Welded Joints Using EBW and GMAW,” *Metals (Basel)*, vol. 12, no. 4, Apr. 2022, doi: 10.3390/met12040678.

[12] R. P. S. Sisodia, M. Gáspár, B. Fodor, and L. Draskóczi, “Simulation and Experimental Based Analysis of the Laser Beam Welding of DP Steels,” *Adv Mat Res*, vol. 1157, pp. 73–82, Feb. 2020, doi: 10.4028/www.scientific.net/amr.1157.73.

[13] M. Tisza, “Advanced materials in sheet metal forming,” in *Key Engineering Materials*, Trans Tech Publications Ltd, 2014, pp. 137–142. doi: 10.4028/www.scientific.net/KEM.581.137.

[14] R. Sisodia, M. Gáspár, and N. Guellouh, “HAZ Characterization of Automotive DP Steels by Physical Simulation,” *International Journal of Engineering and Management Sciences (IJEMS)*, vol. 4, no. 1, 2019, doi: 10.21791/IJEMS.2019.1.59.

[15] P. Kah, M. Pirinen, R. Suoranta, and J. Martikainen, “Welding of ultra high strength steels,” in *Advanced Materials Research*, 2014, pp. 357–365. doi: 10.4028/www.scientific.net/AMR.849.357.

[16] P. C. Huan *et al.*, “Effect of different excitation currents on droplet transfer and weld formation of Al-Mg-Si alloy CMT MIX + Synchropulse welded joint,” *Mater Lett*, vol. 301, Oct. 2021, doi: 10.1016/j.matlet.2021.130311.

[17] M. Chen, D. Zhang, and C. Wu, “Current waveform effects on CMT welding of mild steel,” *J Mater Process Technol*, vol. 243, pp. 395–404, May 2017, doi: 10.1016/j.jmatprotec.2017.01.004.

[18] Q. Sun, J. Li, Y. Liu, Y. Jiang, K. Kang, and J. Feng, “Arc characteristics and droplet transfer process in CMT welding with a magnetic field,” *J Manuf Process*, vol. 32, pp. 48–56, Apr. 2018, doi: 10.1016/j.jmapro.2018.01.017.

[19] A. Elrefaey and N. G. Ross, “Microstructure and mechanical properties of cold metal transfer welding similar and dissimilar aluminum alloys,” *Acta Metallurgica Sinica (English Letters)*, vol. 28, no. 6, pp. 715–724, Jun. 2015, doi: 10.1007/s40195-015-0252-6.